Estimation of peak electron density in upper ionosphere of Mars at high latitude (50°–70°N) using MGS ACC data

S. P. Seth,[1,2] U. B. Jayanthi,[1] and S. A. Haider[3]

Received 31 May 2006; revised 29 August 2006; accepted 1 September 2006; published 13 October 2006.

[1] Under photochemical equilibrium condition, electron density near peak varies as the square root of total peak ionization rate. Thus by averaging the longitudinal variation of latter, the mean primary and secondary peak electron densities in upper ionosphere of Mars using measured mass densities at LST 16 hrs are estimated to be $\sim 8.56 \times 10^4$ cm^{-3} and $\sim 1.81 \times 10^4$ cm^{-3}. On comparison with mean electron densities at LST 3–4 hrs for observational period Dec. 24–31, 1998, at same solar zenith angle, it is found that the estimated primary peak electron density at LST 16 hrs is more by a factor of ~ 1.06. With this analogy, the estimated secondary peak electron density should be $\sim 3.76 \times 10^4$ cm^{-3} instead of $\sim 1.81 \times 10^4$ cm^{-3}. Thus, in order to obtain the estimated secondary peak electron density of $\sim 3.76 \times 10^4$ cm^{-3}, soft X-ray flux should be increased by a factor of ~ 4.31. **Citation:** Seth, S. P., U. B. Jayanthi, and S. A. Haider (2006), Estimation of peak electron density in upper ionosphere of Mars at high latitude (50°–70°N) using MGS ACC data, *Geophys. Res. Lett.*, *33*, L19204, doi:10.1029/2006GL027064.

1. Introduction

[2] Mars Global Surveyor (MGS) was launched in November 1996 and reached Mars in September 1997. The orbit of MGS was altered using the technique of aerobraking. In this technique, the atmosphere of the planet is used instead of fuel to obtain the desired orbit. Aerobraking on MGS took place in two phases, 1 and 2, separated by a hiatus containing the Science Phasing Orbits [*Albee et al.*, 2001]. The orbit of MGS during aerobraking was near-polar and highly elliptical, with an inclination of about 93°.

1.1. Accelerometer Instrument

[3] The Accelerometer Experiment (ACC) onboard MGS measured many mass density profiles in the upper atmosphere of Mars during aerobraking at many latitudes, longitudes, altitudes, local solar time (LST) and seasons [*Withers et al.*, 2003]. Aerobraking took place in two phases, 1 and 2. Phase 1 included the orbits from # P1-P201 from mid September 1997, to late March 1998, while Phase 2 included the orbits from # P574-P1283 from mid September 1998, to early February 1999. The maximum altitude at which the accelerometer measured thermospheric density as set by the sensitivity of the instrument was 160 km. The minimum altitude at which it measured the thermospheric density was that of periapsis, which is rarely outside 100–120 km. A given altitude level was crossed twice on each aerobraking pass, one descending towards periapsis and another ascending after the periapsis, both at different sets of latitude and longitude. These two measurements at same altitude and same orbit are distinguished by referring them as "inbound" and "outbound" legs of an aerobraking pass.

[4] The MGS accelerometer data have been used for studies of global features and dynamical properties of neutral atmosphere [*Keating et al.*, 1998; *Tolson et al.*, 1999; *Bougher et al.*, 2001, 2004; *Withers*, 2006; *Withers et al.*, 2003]. The analysis of these aerobraking data sets confirms a strong coupling of the lower and upper atmosphere of Mars [*Bougher et al.*, 2006, and references therein]. Here, in this paper, we use the accelerometer data of 57 orbits (#P0588 – P0648) between latitude ranges (50°–70°N) from September 30, 1998 to October 24, 1998, under spring equinox and medium solar activity conditions (average $F_{10.7} \sim 120$) during phase 2 of the aerobraking. During these orbits, the Martian heliocentric longitude L_s is from 34°–45°, solar zenith angle (SZA) is from 56°–66° and local solar time (LST) is 16 hrs.

1.2. Radio Occultation Instrument

[5] The radio occultation technique can be used to probe the neutral and plasma structure of the Mars atmosphere. Radio science (RS) instrument onboard MGS employs an ultra-stable radio oscillator. The signal from the oscillator to Earth is refracted by the Martian atmosphere, allowing the retrieval of neutral temperature profiles (0–50 km) and electron density profiles (~95–200 km) [*Tyler et al.*, 2001]. Thus radio occultation technique monitors the characteristics of lower and upper atmospheres of Mars. *Hinson et al.* [2001], reviews the occultation technique and describes the RS measurements conducted in late 1998 during phase 2 of aerobraking. Until now, the MGS RS experiment team has so far released four data sets namely EDS1, EDS2, EDS3 and EDS4 to the scientific community [*Bougher et al.*, 2004]. *Bougher et al.* [2001] examined the initial set of RS 32 electron density profiles of EDS1 data set. The solar zenith angle (SZA) of the observed electron density profiles during the EDS1 data set is from 78°–81°. By averaging all SZA and longitude variations of EDS1 data set, the mean primary and secondary peak electron densities are estimated as $\sim 8.1 \times 10^4$ cm^{-3} and $\sim 3.55 \times 10^4$ cm^{-3} at mean height of 134.4 km and 112 km respectively. Table 1 summarizes the RS and ACC data sets and gives the dates and associated parameters for our present investigation. Recently, the radio science experiment on the European Mars Express spacecraft observed a third ionospheric layer at altitude ranges of 65 to 110 km

[1] Instituto Nacional de Pesquisas Espaciais, INPE, Sao Jose dos Campos, Sao Paulo, Brazil.
[2] Also at Bhavan's Ranchhodlal Acharatlal College of Science, Gujarat University, Ahmedabad, India.
[3] Physical Research Laboratory, Navrangpura, Ahmedabad, India.

0094-8276/06/2006GL027064

Table 1. Parameters of MGS RS/ACC Data Set

Type of Data	Dates	Orbit	Ls	LST	SZA (LAT)
RS	24–31 Dec, 1998 (EDS1)	917–963 (32)	74° – 77°	3–4 hrs	78°–81° (64.7°–67.3°N)
ACC	30 Sept–24 Oct, 1998	#P0588 #P0648 (57)	34° – 45°	16 hrs	56°–66° (50°–70° N)

with a peak magnitude of $\sim 8 \times 10^3$ cm^{-3} [*Patzold et al.*, 2005]. The origin of this third layer has been attributed due to the ablation of meteors and charge exchange of magnesium and iron.

[6] This paper has two objectives: (1) Using accelerometer data of 57 orbits (#P0588 – P0648) between latitude ranges (50°–70°N) under spring equinox and medium solar activity conditions (average $F_{10.7} \sim 120$) during phase 2 of the aerobraking, we calculate the longitudinal distribution of total peak ionization (Photoionization + Photoelectron impact ionization) rates and their peak altitude due to absorption of solar EUV and soft X-ray (1–102.57 nm) radiation; longitudinal distribution of electron impact ionization rates due to absorption of soft X-ray (1–9 nm) radiation only and their peak altitude. These calculations are carried out at different altitudes and longitudes starting from 115 km to 220 km and from 0°E to 360°E at the intervals of 0.1 km and 5° respectively for solar zenith angle 78° using Analytical Yield Spectrum (AYS) Approach. (2) Under photochemical equilibrium condition, the electron density near the peak varies as the square root of the total peak ionization rate. Thus, by washing out all longitudinal variations of calculated total peak ionization rates, we estimate the magnitude of primary and secondary peak electron densities using the measured mass densities for the observational period September 30, 1998 to October 24, 1998, between latitude ranges (50°–70°N) at LST 16 hrs, under spring equinox and medium solar activity conditions. These estimated mean primary and secondary peak electron densities are then compared with the mean electron densities obtained by washing out all longitudinal variations of the 32-electron density profiles for the latitude (64.7°–67.3°N) at LST 3–4 hrs in the early morning for the observational period Dec. 24–31, 1998 during solar moderate conditions. It must be emphasized here, that both the observations and the calculations are done at same solar zenith angle.

2. Calculation and Input Parameters

[7] The mass density from accelerometer experiment, between latitude (50°–70°N), for the orbits #P0588 to #P0648 (57 orbits) from September 30, 1998 to October 24, 1998 during early northern spring is available only from 115 km and up to 160 km. At that time, the Northern hemisphere of Mars had spring season (Ls = 34°– 45°) with moderate solar activity. The neutral densities of five main atmospheric constituents namely CO_2, N_2, O_2, O and CO are derived from 115 km to 160 km and from 0° E to 360° E at the interval of 0.1 km and 5° respectively by multiplying the mixing ratios of these gases with the mass densities. The mixing ratios are adopted from *Bougher et al.* [2000] and *Fox* [1997] at different altitudes for similar conditions of MGS phase 2 aerobraking period. Since the accelerometer experiment measured the mass density up to 160 km, and for the correct calculations of solar photon attenuation down to the photochemical regime we need the neutral densities above 160 km, so above 160 km and up to 220 km the neutral densities are taken from *Bougher et al.* [2000].

[8] The branching ratios, photoabsorption and photoionization cross sections are taken from other references [e.g., *Raina and Haider*, 1998; *Seth*, 2003]. The solar flux is taken from SOLAR 2000 model [*Tobiska et al.*, 2000] which is an empirical model of the full solar spectrum drawing ground-based and satellite measurements available for each day. The flux emitted from a region of the Sun varies with time and position on the solar disk i.e. solar flux varies with solar latitude and longitude as well as time. The corrections in the solar flux are made for the varying distances of Earth and Mars from the Sun, and for variations in the Earth-Sun-Mars angle as the planets orbit around the Sun. With respect to the latter, at Mars the flux from the Sun is shifted in time from that observed at Earth by an amount determined by the Earth-Sun-Mars angle, and the rotation period of the Sun [*Withers and Mendillo*, 2005; *Bruinsma et al.*, 2006; *Breus et al.*, 2004]. The Earth-Sun-Mars angle was −115° on September 30, 1998 and it decreases monotonically to −103° on October 24, 1998. These positions correspond to timeshifts of 9 and 8 days respectively. Here we adopt the convention that Earth-Sun-Mars angles are negative, when the Earth is trailing Mars (i.e., prior to opposition) and positive when Mars is trailing Earth (i.e., after opposition). The solar flux is scaled by $1/R^2$ where R is heliocentric distance equal to 1.644 AU, appropriate for accelerometer experiment for the above mentioned period during MGS-Phase 2 aerobraking period.

[9] The linear interpolation method is used wherever accelerometer data of mass density with respect to longitude is not available at these intervals. The distribution of photoionization rate at different altitude and longitude is calculated at solar zenith angle 78°, same as that of the observation of EDS1 data set, by using formula as given by *Bhardwaj* [2003] and *Seth et al.* [2006]. The variation of photoionization rate with altitude indicates the presence of two peaks namely primary and secondary peak. The primary peak is mostly due to the absorption of solar ultraviolet radiation between 20 nm and 90 nm, while the photons with wavelengths shorter than 20 nm are absorbed below this primary peak. The photoelectron impact ionization rates are calculated using two dimensional analytical yield spectrum approach as described in our previous papers [*Haider et al.*, 2006; *Seth et al.*, 2006, 2002; *Haider and Bhardwaj*, 2005, and references therein]. This approach is useful in the lower thermosphere ($\leq$ 200 km) where vertical transport of photoelectron is not allowed. To save the computational time for the calculation of photoelectron impact ionization rates, the energy grids of width 2 eV between 0 and 10 eV and a width of 2.5 eV between 10–1000 eV is chosen.

3. Results and Discussion

[10] Figure 1 represents the distribution of mass density at reference altitudes of 130, 140, 150 and 160 km versus

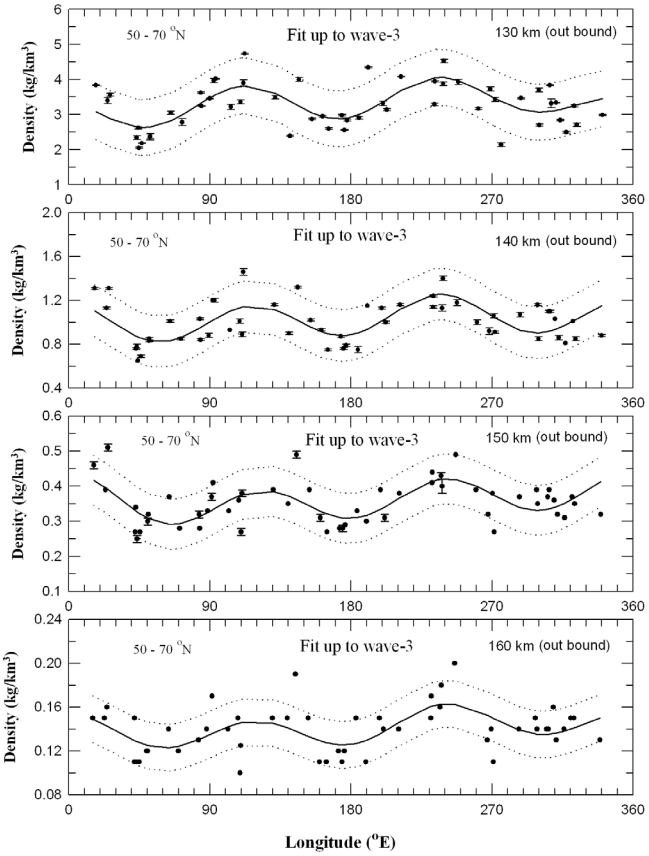

Figure 1. MGS accelerometer data of mass density for latitude range 50°–70°N from altitudes 130 km and160 km. Solid line indicates the best fit to data and dotted line represent 0.95 prediction confidence limits.

longitude for the outbound leg of orbits #P0588–P0648 (57 orbits) between latitude ranges (50°–70°N). These mass densities are measured by MGS accelerometer experiment from September 30, 1998 to October 24, 1998, under spring equinox and medium solar activity conditions (average $F_{10.7} \sim 120$) during phase 2 of the aerobraking. Initially *Keating et al.* [1998] suggested that this zonal variation is due to topographically forced stationary waves. But later it has been shown that this is due to the presence of thermal tides [*Keating et al.*, 2001; *Forbes and Hagan*, 2000; *Joshi et al.*, 2000; *Wilson*, 2002]. Thermal tides are planetary-scale waves with periods that are harmonics of the solar day. These include westward propagating, migrating (sun-synchronous) waves forced in response to solar heating, and additional nonmigrating waves resulting from the zonal variations in the thermotidal forcing. Thus, the mass density measurements indicate the presence of planetary-scale wave structure and tidal waves in the upper atmosphere of Mars [*Hinson et al.*, 2001; *Wilson*, 2002]. These types of waves arise in response to surface forcing [e.g., *Hollingsworth and Barnes*, 1996; *Barnes et al.*, 1996; *Nayvelt et al.*, 1997; *Wilson and Richardson*, 2000].

[11] Measurement uncertainties are also shown in Figure 1, which are much smaller than the range in multiple measurements at any longitude. We use a least square fit up to wave-3 (wave 1, 2, plus 3) harmonic model to characterize the zonal structure as shown in Figure 1 [*Withers et al.*, 2003; *Krymskii et al.*, 2003; *Bougher et al.*, 2001]. This model contains a constant density term, an amplitude and phase for a sinusoid with one cycle per 360° of longitude, which is labeled as wave-1 harmonic, and higher harmonics up to and including wave-3. It has seven free parameters. In Figure 1, the solid and dotted lines are plotted for model fit values and 0.95 confidence limit respectively. The zonal structure with large peaks in density at ∼100° −140° E, ∼220° −260° E and ∼340° −20° E can be seen. Also it can be seen from Figure 1 that the zonal structure which is present between 130 and 160 km, decays with increasing altitude.

[12] *Haider et al.* [2002] studied the possible sources of primary and secondary ionization in the dayside ionosphere of Mars. They concluded that in the dayside ionosphere of Mars, the primary peak is produced by photoionization and photoelectron impact ionization processes due to the absorption of solar EUV and soft X-ray radiation (1–102.57 nm) while the secondary peak is controlled by the electron impact ionization of soft X-ray radiation (1–9 nm). Thus the longitudinal distribution of total peak ionization

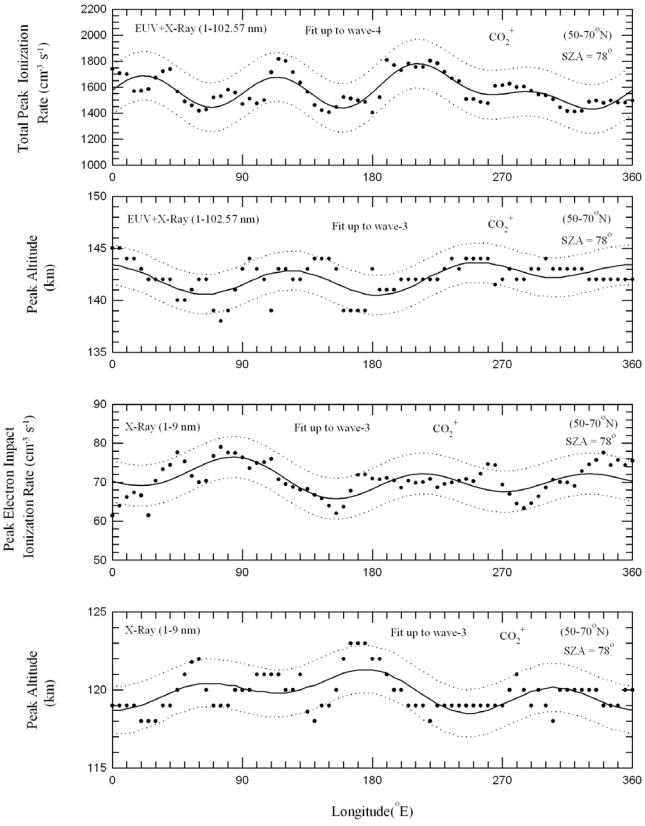

Figure 2. The longitudinal variation of total peak ionization (Photoionization + Photoelectron impact ionization) rates of CO_2^+ due to absorption of solar EUV and soft X-ray (1–102.57 nm) radiation and their peak altitude for latitude range 50°–70°N; the longitudinal variation of electron impact ionization rates of CO_2^+ due to absorption of soft X-ray (1–9 nm) radiation only and their peak altitude for latitude range 50°–70°N are shown. Solid line indicates the best fit to data and dotted line represent 0.95 prediction confidence limits.

(Photoionization + Photoelectron impact ionization) rates of CO_2^+ due to absorption of solar EUV and soft X-ray (1–102.57 nm) radiation and their peak altitude; the longitudinal distribution of electron impact ionization rates of CO_2^+ due to absorption of soft X-ray (1–9 nm) radiation only and their peak altitude are shown in Figure 2. These calculations are carried out at different altitudes and longitudes starting from 115 km to 220 km and from 0°E to 360°E at the intervals of 0.1 km and 5° respectively for solar zenith angle 78° using Analytical Yield Spectrum (AYS) Approach [*Seth*, 2003]. The total ionization rates of other gases like N_2^+, O_2^+, O^+ and CO^+ are also calculated, but they are not shown in the Figure 2. As it is seen from Figure 2 that total peak ionization (Photoionization + Photoelectron impact ionization) rates and the peak altitudes of CO_2^+ due to absorption of solar EUV and soft X-ray (1–102.57 nm) radiation are fitted with a harmonic up to wave-4 and wave-3 harmonic model which has 9 and 7 free parameters respectively. Similarly the peak electron impact ionization rates due to absorption of soft X-ray (1–9 nm) radiation only and their corresponding peak altitudes are fitted with a harmonic up to wave-3 harmonic model which has 7 free parameters shown in Figure 2. The solid and dotted lines are plotted for model fit values and 0.95 confidence limit respectively.

[13] The zonal structure of peak altitude of total peak ionization (Photoionization + Photoelectron impact ionization) rates of CO_2^+ due to absorption of solar EUV and soft X-ray (1–102.57 nm) radiation shows maxima at 100°–145°E, 220°–280°E and 340°–30°E about a statistical mean of 142.2 km. Similarly, the zonal structure of peak altitude of peak electron impact ionization rates due to absorption of soft X-ray (1–9 nm) radiation only shows maxima at ~119.8 km (~22.4 km lower) and these maxima are shifted westward by ~55°. The calculated longitude variations in peak altitude of total peak ionization rates correspond to the measured mass density variations, while the peak altitude of the peak photoelectron impact ionization rate is out of phase with the mass density variations.

[14] Under the photochemical equilibrium condition the electron density near the peak varies as the square root of their total peak ionization rate. The mean peak electron density in the high latitude ionosphere can be estimated as $n_e(h_m) \approx \mathrm{sqrt}\{q(h_m)/\alpha\}$, where $q(h_m)$ is the total peak ionization rate of CO_2^+ taken from Figure 2 at mean peak altitude h_m and $\alpha = 1.9 \times 10^{-7}(300/T_e)^{0.7}$ cm^3s^{-1} [*Schunk and Nagy*, 2000]. The value of T_e is taken as 261°K from *Bougher et al.* [2000] at northern summer solstice (NSLMED) at northern mid latitude region. Thus, by washing out all longitudinal variations of calculated total peak ionization rates, the primary and secondary peak electron densities are estimated to be $\sim 8.56 \times 10^4$ cm^{-3} and $\sim 1.81 \times 10^4$ cm^{-3} using the measured mass densities at LST 16 hrs. These estimated peak electron densities are then compared with mean primary and secondary electron densities of $\sim 8.1 \times 10^4$ cm^{-3} and $\sim 3.55 \times 10^4$ cm^{-3} obtained by washing out all longitudinal variations of RS EDS1 data set at LST 3–4 hrs. The estimated primary peak electron density at LST 16 hrs is more by a factor of ~1.06 than the observed primary peak electron density at LST 3–4 hrs. With this analogy, the estimated secondary peak electron density at LST 16 hrs should be $\sim 3.76 \times 10^4$ cm^{-3} instead of $\sim 1.81 \times 10^4$ cm^{-3}. Thus, in order to obtain the estimated secondary peak electron density of $\sim 3.76 \times 10^4$ cm^{-3} at LST 16 hrs, under spring equinox and medium solar activity conditions (average $F_{10.7} \sim 120$) the soft X-ray flux should be increased by a factor of ~ 4.31. This is in good agreement with the model calculation of *Fox* [2004], who found that for low and high solar activity, the lower peak increases by a factor of ~3.0 and ~ 6.0 from the standard to enhanced X-ray models.

4. Conclusions

[15] Using the density profiles of the Mars upper atmosphere, measured with the accelerometer of MGS, as shown in Table 1, the longitudinal distribution of total peak ionization (Photoionization + Photoelectron impact ionization) rates, due to absorption of solar EUV and soft X-ray (1–102.57 nm) radiation; electron impact ionization rates due to absorption of soft X-ray (1–9 nm) radiation only and their corresponding peak altitudes are obtained at high latitude range (50°–70°N). By washing out all longitudinal variations of calculated total peak ionization rates, the magnitudes of primary and secondary peak electron densities are estimated at same SZA, using the measured mass densities for the latitude (50°–70°N) at LST 16 hrs. These estimated mean primary and secondary peak electron densities are then compared with the mean electron densities obtained from the 32-electron density profiles for the latitude (64.7°–67.3°N) at LST 3–4 hrs in the early morning for the observational period Dec. 24–31, 1998 during solar moderate conditions. The estimated primary peak electron density at LST 16 hrs is more by a factor of ~1.06 than the estimated primary peak electron density at LST 3–4 hrs. With this analogy, the estimated secondary peak electron density at LST 16 hrs should be ~3.76 x 10^4 cm^{-3} instead of $\sim 1.81 \times 10^4$ cm^{-3}. Thus, in order to obtain the estimated secondary peak electron density of $\sim 3.76 \times 10^4$ cm^{-3} at LST 16 hrs, under spring equinox and medium solar activity conditions the soft X-ray flux should be increased by a factor of ~ 4.31 which is in good agreement with the model calculation of *Fox* [2004], who found that for low and high solar activity, the lower peak increases by a factor of ~3.0 and ~ 6.0 from the standard to enhanced X-ray models. This method of obtaining peak electron densities from the measured mass densities is going to be helpful for those future Mars Planetary missions having no radio science experiment.

[16] **Acknowledgments.** The authors thank Dave Hinson and the MGS Radio Science Team for providing us the electron density data. The authors are also thankful to G. M. Keating, George Washington University, NASA Langley, Hampton, USA and his group for providing us accelerometer data through NASA Planetary Data System 2001. S. P. S. thanks CNPq for the fellowship. In addition, we thank two anonymous reviewers for their constructive comments for improving this manuscript.

References

Albee, A. L., R. E. Arvidson, F. Palluconi, and T. Thorpe (2001), Overview of Mars Global Surveyor mission, *J. Geophys. Res.*, *106*, 23,291.

Barnes, J. R., R. M. Haberle, J. B. Pollack, H. Lee, and J. Schaeffer (1996), Mars atmospheric dynamics as simulated by the NASA Ames General Circulation Model: 3. Winter quasistationary eddies, *J. Geophys. Res.*, *101*, 12,753.

Bhardwaj, A. (2003), On the solar EUV deposition in the inner comae of comets with large gas production rates, *Geophys. Res. Lett.*, *30*(24), 2244, doi:10.1029/2003GL018495.

Bougher, S. W., S. Engel, R. G. Roble, and B. Foster (2000), Comparative terrestrial planet thermospheres: 3. Solar cycle variation of global structure and winds at solstices, *J. Geophys. Res.*, *105*, 17,669.

Bougher, S. W., S. Engel, D. P. Hinson, and J. M. Forbes (2001), Mars Global Surveyor Radio Science electron density profiles: Neutral atmosphere implications, *Geophys. Res. Lett.*, *28*, 3091.

Bougher, S. W., S. Engel, D. P. Hinson, and J. R. Murphy (2004), MGS Radio Science electron density profiles: Interannual variability and implications for the Martian neutral atmosphere, *J. Geophys. Res.*, *109*, E03010, doi:10.1029/2003JE002154.

Bougher, S. W., J. M. Bell, J. R. Murphy, M. A. Lopez-Valverde, and P. G. Withers (2006), Polar warming in the Mars thermosphere: Seasonal variations owing to changing insolation and dust distributions, *Geophys. Res. Lett.*, *33*, L02203, doi:10.1029/2005GL024059.

Breus, T. K., A. M. Krymskii, D. H. Crider, N. F. Ness, D. Hinson, and K. K. Barashyan (2004), Effect of the solar radiation in the topside atmosphere/ionosphere of Mars: Mars Global Surveyor observations, *J. Geophys. Res.*, *109*, A09310, doi:10.1029/2004JA010431.

Bruinsma, S., J. M. Forbes, and F. Lemoine (2006), Solar flux variability and Mars thermosphere densities derived from orbital tracking data, paper presented at Second Mars Atmosphere Modeling and Observations Workshop, Inst. de Astrofis. de Andalucia, Granada, Spain.

Forbes, J. M., and M. E. Hagan (2000), Diurnal Kelvin wave in the atmosphere of Mars: Towards an understanding of "stationary" density structures observed by the MGS accelerometer, *Geophys. Res. Lett.*, *27*, 3563.

Fox, J. L. (1997), Upper limits to the outflow of ions at Mars: Implications for atmospheric evolution, *Geophys. Res. Lett.*, *24*, 2901.

Fox, J. L. (2004), Response of the Martian thermosphere/ionosphere to enhanced fluxes of solar soft X rays, *J. Geophys. Res.*, *109*, A11310, doi:10.1029/2004JA010380.

Haider, S. A., and A. Bhardwaj (2005), Radial distribution of production rates, loss rates and densities corresponding to ion masses $\leq$40 amu in the inner coma of comet Halley: Composition and chemistry, *Icarus*, *177*, 196.

Haider, S. A., S. P. Seth, E. Kallio, and K. I. Oyama (2002), Solar EUV and electron-proton-hydrogen atom-produced ionosphere on Mars: Comparative studies of particle fluxes and ion production rates due to different processes, *Icarus*, *159*, 18.

Haider, S. A., S. P. Seth, V. R. Choksi, and K. I. Oyama (2006), Model of photoelectron impact ionization within the high latitude ionosphere at Mars: Comparison of calculated and measured electron density, *Icarus*, doi:10.1016/j.icarus.2006.07.010.

Hinson, D. P., G. L. Tyler, J. L. Hollingsworth, and R. J. Wilson (2001), Radio occultation measurements of forced atmospheric waves on Mars, *J. Geophys. Res.*, *106*, 1463.

Hollingsworth, J. L., and J. R. Barnes (1996), Forced stationary planetary waves in Mars' winter atmosphere, *J. Atmos. Sci.*, *53*, 428.

Joshi, M. M., J. L. Hollingsworth, R. H. Haberle, and A. F. C. Bridger (2000), An interpretation of Martian thermospheric waves based on analysis of a general circulation model, *Geophys. Res. Lett.*, *27*, 613.

Keating, G.M., et al. (1998), The structure of the upper atmosphere of Mars: In-situ accelerometer measurements from Mars Global Surveyor, *Science*, *279*, 1672.

Keating, G. M., R. H. Tolson, A. M. Dwyer, S. W. Bougher, P. G. Withers, and J. M. Forbes (2001), Persistent planetary-scale wave-2 and wave-3 density variations observed in Mars upper atmosphere from MGS accelerometer experiment, *Proc. Eur. Geophys. Soc.*, *78*, 229.

Krymskii, A. M., T. K. Breus, N. F. Ness, D. P. Hinson, and D. I. Bojkov (2003), Effects of crustal magnetic fields on the near terminator ionosphere at Mars: Composition of in situ magnetic field measurements with the data of radio science experiments on board Mars Global Surveyor, *J. Geophys. Res.*, *108*(A12), 1431, doi:10.1029/2002JA009662.

Nayvelt, L., P. J. Gierasch, and K. H. Cook (1997), Modeling and observations of Martian stationary waves, *J. Atmos. Sci.*, *54*, 986.

Patzold, M., et al. (2005), A sporadic third layer in the ionosphere of Mars, *Science*, *310*, 837.

Raina, K. S., and S. A. Haider (1998), Chemistry of the dayside ionosphere of Mars, *Indian J. Radio Space Phys.*, *27*, 185.

Schunk, R. W., and A. F. Nagy (2000), *Ionospheres*, Cambridge Univ. Press, New York.

Seth, S. P. (2003), Solar wind interaction with planets, Ph. D. thesis, Gujarat Univ., Ahmedabad, India.

Seth, S. P., S. A. Haider, and K. I. Oyama (2002), The photoelectron flux and nightglow emissions of 5577 A and 6300 A due to solar wind electron precipitation in Martian atmosphere, *J. Geophys. Res.*, *107*(A10), 1324, doi:10.1029/2001JA000261.

Seth, S. P., V. Brahmananda Rao, C. M. Esprito Santo, S. A. Haider, and V. R. Choksi (2006), Zonal variations of peak ionization rates in upper atmosphere of Mars at high latitude using Mars Global Surveyor accelerometer data, *J. Geophys. Res.*, *111*, A09308, doi:10.1029/2006JA011753.

Tobiska, W. K., T. Woods, F. Eparvier, R. Viereck, L. Floyd, D. Bouwer, G. Rottman, and O. R. White (2000), The SOLAR 2000 empirical solar irradiance model and forecast tool, *J. Atmos. Sol. Terr. Phys.*, *62*, 1233.

Tolson, R. H. (1999), Utilization of Mars Global Surveyor accelerometer data for atmospheric modeling, paper presented at Astrodynamics Specialist Conference, Am. Astrodyn. Soc., Girdwood, Alaska.

Tyler, G. L., G. Balmino, D. P. Hinson, W. L. Sjogren, D. E. Smith, R. A. Simpson, S. W. Asmar, P. Priest, and J. D. Twicken (2001), Radio Science observations with Mars Global Surveyor: Orbit insertion through one Mars year in mapping orbit, *J. Geophys. Res.*, *106*, 23,327.

Wilson, R. J. (2002), Evidence for nonmigrating thermal tides in the Mars upper atmosphere from the Mars Global Surveyor accelerometer experiment, *Geophys. Res. Lett.*, *29*(7), 1120, doi:10.1029/2001GL013975.

Wilson, R. J., and M. I. Richardson (2000), The Martian atmosphere during the Viking mission: 1. Infrared measurements of atmospheric temperatures revisited, *Icarus*, *145*, 555.

Withers, P. (2006), Mars Global Surveyor and Mars Odyssey Accelerometer observations of the Martian upper atmosphere during aerobraking, *Geophys. Res. Lett.*, *33*, L02201, doi:10.1029/2005GL024447.

Withers, P., and M. Mendillo (2005), Response of peak electron densities in the Martian ionosphere to day-to-day changes in solar flux due to solar rotation, *Planet. Space Sci.*, *53*, 1401.

Withers, P., S. W. Bougher, and G. M. Keating (2003), The effects of topographically controlled thermal tides in the Martian upper atmosphere, *Icarus*, *164*, 14.

S. A. Haider, Physical Research Laboratory, Navrangpura, Ahmedabad, India. (haider@prl.res.in)

U. B. Jayanthi and S. P. Seth, Instituto Nacional de Pesquisas Espaciais, INPE, Sao Jose dos Campos, 1758 Avenida dos Astronautas, SP 12201-970, Brazil. (jayanthi@das.inpe.br; sseth@das.inpe.br)